

Diffracting and Non-diffracting random fields

Patnala Vanitha¹, Bhargavi M¹, Venkateswarlu Annapureddy^{2,*}, Gangi Reddy Salla^{1,**}, Yoko Miyamoto^{3,4}, and R. P. Singh⁵

¹Department of Physics, SRM University-AP, Andhra Pradesh, India - 522240.

²Department of Physics, National Institute of Technology Tiruchirappalli, Tamil Nadu 620015, India.

³Department of Engineering Science, The University of Electro-Communications, Chofugaoka, Chofu, Tokyo 1828585, Japan.

⁴Institute for Advanced Science, The University of Electro-Communications, Chofugaoka, Chofu, Tokyo 1828585, Japan.

⁵Physical Research laboratory, Navarangpura, Ahmedabad, India-380009.

**Corresponding author: gangireddy.s@srmmap.edu.in

ABSTRACT

We have generated and propagated both diffracting and non-diffracting speckles using the scattering of perfect optical vortices. The diffracting speckles have been realized in the near field and non-diffracting speckles have been realized in the far field, that is after taking the Fourier transform of near-field speckles using a simple convex lens. The exact analytical expressions have been provided for the size of both diffracting as well as non-diffracting speckles and compared with our experimental results. We found that the experimental results are in good agreement with the theoretical results. These results may find applications in classical cryptography and communication as we have both varying and non-varying random field patterns with propagation distance.

1 Introduction

Optical vortices have helical wave fronts due to their azimuthal phase along with a singularity at the center¹. They carry an orbital angular momentum (OAM) of $m\hbar$ per photon, m being the order of the vortex^{2,3}. These beams have attracted a lot of interest due to their applications in science and technology^{4,5}. Recently, a new class of vortex beams have been introduced, namely perfect optical vortices (POV), which have order independent intensity distributions⁶. The POV beams can be generated using various techniques such as the Fourier transform of Bessel-Gauss (BG) beams⁷⁻¹⁰. Here, we have utilized the scattering of the POV beams for generating the diffracting as well as non-diffracting random patterns.

Speckle is a random granular light pattern and formed when a rough surface such as ground glass plate is illuminated by a coherent light beam^{11,12}. This random pattern is due to the interference of scattered wave fronts arriving from a large number of inhomogeneities present in the rough surface¹³⁻¹⁶. These random patterns have significant applications in science and technology such as communication and cryptography¹⁷⁻²⁴. It has been observed that when optical vortices are scattered through a rough surface, the speckle size decreases with the increase in order¹¹.

Since POV beams have order independent intensity distributions, it is of interest whether they produce order dependent speckles when scattered. We have previously scattered POV beams and found that the resulting speckle size, defined as the spatial length up to which the field is correlated, is independent of the order of the POV beams²⁵. We have further studied these speckles in the far field, i.e., through a Fourier transforming lens, and found that they were non-diffracting^{26,27}. The size of the speckles can be controlled by changing the axicon parameter used in the generation of POV beams. We have also reported the generation of Bessel-Gauss coherence functions using the speckles obtained by scattering POV beams²⁸. While the speckle size in the far field is order independent, the speckle pattern itself is altered by the vortex, leading to specific cross-correlation functions dependent on the combination of POV orders.

In this work we examine in detail the change of speckle size during propagation and confirm that both diverging as well as non-diverging speckles can be generated from POV beams. As before the far field speckles are obtained by taking the Fourier transform of near field speckles using a plano-convex spherical lens. We derive the exact analytical expressions for the size of both near and far field speckles using the auto-correlation function. The size of near field speckles varies linearly with propagation distance and the size of far field speckles is independent of the propagation distance. We also verify our theoretical results experimentally for the near field and far field speckles.

2 Theoretical Analysis

Let us consider the field distribution of a perfect optical vortex (of order m) beam, which can be expressed as⁷

$$E(\rho, \theta) = \delta(\rho - \rho_0) e^{im\theta} \quad (1)$$

where ρ_0 is the radius of the POV beam, and δ indicates the Dirac delta function. To allow for the POV beams having finite width ε , we replace the delta function with a narrow-Gaussian function $g(\rho - \rho_0; \varepsilon)$ so that

$$E(\rho, \theta) = g(\rho - \rho_0; \varepsilon) e^{im\theta} \quad (2)$$

In order to realize the diffracting and non-diffracting speckles, we propagate the POV beams through a rough surface, such as a ground glass plate (GGP). The theoretical formulation for the scattering of light beams through a GGP can be done using a random phase function $e^{i\Phi}$, where Φ is a random phase that varies in the range 0 to 2π . Now, the scattered field distribution is given by¹³

$$U(\rho, \theta) = e^{i\Phi(\rho, \theta)} E(\rho, \theta) \quad (3)$$

The inhomogeneities present in a ground glass plate are independent of each other and their size is of the order of $20 \mu m$, which is very small compared to typical beam size. This implies that the auto-correlation of the phase exponential factor present in the above equation 3 is provided by a Dirac-delta function as given below:

$$\langle e^{i[\Phi(\rho_1, \theta_1) - \Phi(\rho_2, \theta_2)]} \rangle = \delta(\rho_1 - \rho_2) \delta(\theta_1 - \theta_2) \quad (4)$$

where $\langle a \rangle$ denote the ensemble average operation on a ²⁹.

The speckle size can be determined using the width of the auto-correlation function of a given speckle pattern. The autocorrelation function of a scattered field at a given plane (z) is defined as¹³

$$\Gamma(r_1, \varphi_1; r_2, \varphi_2) = \langle U_1(r_1, \varphi_1, z) U_2^*(r_2, \varphi_2, z) \rangle \quad (5)$$

For finding the speckle size for different propagation distances, we evaluate the above equation using Fresnel diffraction integral, which can be written in cylindrical coordinates as³⁰,

$$\Gamma_{12}(\Delta r) = \frac{e^{\frac{ik}{2z}(r_1^2 - r_2^2)}}{\lambda^2 z^2} \int \int |U_1(\rho, \theta)|^2 e^{-\frac{ik}{z}(\rho \Delta r \cos(\varphi_s - \theta))} \rho d\rho d\theta \quad (6)$$

where

$$\Delta r \cos(\varphi_s - \theta) = [(r_1 \cos(\varphi_1) - r_2 \cos(\varphi_2)) \cos\theta] + [(r_1 \sin(\varphi_1) - r_2 \sin(\varphi_2)) \sin\theta] \quad (7)$$

and $\Delta r^2 = r_1^2 + r_2^2 - 2r_1 r_2 \cos(\varphi_2 - \varphi_1)$. Note that equation 4 has already been applied.

By using Eq. 3, we get the initial intensity as²⁸

$$\begin{aligned} U(\rho, \theta) U^*(\rho, \theta) &= E(\rho, \theta) e^{i\Phi(\rho, \theta)} E^*(\rho, \theta) e^{-i\Phi(\rho, \theta)} \\ &= E(\rho, \theta) E^*(\rho, \theta) \end{aligned} \quad (8)$$

Using Eq. 2 we obtain

$$E(\rho, \theta) E^*(\rho, \theta) = g(\rho - \rho_0; \varepsilon) g(\rho - \rho_0; \varepsilon) = g^2(\rho - \rho_0; \varepsilon) \quad (9)$$

Under the approximation $\varepsilon \rightarrow 0$, one can replace $g^2(\rho - \rho_0; \varepsilon)$ with a single Dirac-delta function $\delta(\rho - \rho_0)$. By substituting this along with Eqs. 8 and 9 in Eq.6, we get the auto-correlation function as

$$\Gamma_{12}(\Delta r) = \frac{e^{\frac{ik}{2z}(r_1^2 - r_2^2)}}{\lambda^2 z^2} \int \int \delta(\rho - \rho_0) e^{-\frac{ik}{z}(\rho \Delta r \cos(\varphi_s - \theta))} \rho d\rho d\theta \quad (10)$$

Using Anger-Jacobi identity and the integral properties of Dirac-delta function, we obtain the correlation function as³¹

$$\Gamma_{12}(\Delta r) = \frac{2\pi\rho_0 e^{\frac{ik}{2z}(r_1^2 - r_2^2)}}{\lambda^2 z^2} J_0\left(\frac{k\rho_0}{z} \Delta r\right) \quad (11)$$

The above equation contains the zero-order Bessel function of the first kind²⁸. The speckle size is defined as the spatial length up to which correlations exist in the field. Here, we consider the speckle size as the distance of first zero of correlation function from center. The first zero of zeroth order Bessel function function $J_0(x) = 0$ happens at $x = 2.4$ and the correlation length or speckle size can be obtained as

$$\Delta r = \frac{xz}{k\rho_0} = \frac{2.4z}{k\rho_0} \quad (12)$$

It is clear from the above equation that the size of near-field speckles varies linearly with propagation distance z , is independent of order m , and inversely proportional to the ring radius ρ_0 .

The far-field speckle pattern can be obtained by taking the Fourier transform of near-field speckle pattern, which can be realized in the lab using a simple convex lens (L2) of focal length f_2 . The auto-correlation function $\Gamma'_{12}(\Delta r')$ of the far field is³⁰

$$\Gamma'_{12}(\Delta r') = \frac{1}{\lambda^2 f_2^2} \int \int |U(\rho, \theta)|^2 e^{-\frac{ik}{f_2}(\rho \Delta r' \cos(\varphi_s - \theta))} \rho d\rho d\theta \quad (13)$$

where $\Delta r'^2 = r_1'^2 + r_2'^2 - 2r_1'r_2' \cos(\varphi_2' - \varphi_1')$. By substituting the Eqs. 8 and 9 in Eq.13, then we get

$$\Gamma'_{12}(\Delta r') = \frac{1}{\lambda^2 f_2^2} \int \int \delta(\rho - \rho_0) e^{-\frac{ik}{f_2}(\rho \Delta r' \cos(\varphi_s - \theta))} \rho d\rho d\theta \quad (14)$$

Once again the Anger-Jacobi identity and the integral properties of Dirac-delta function give

$$\Gamma'_{12}(\Delta r') = \frac{2\pi\rho_0}{\lambda^2 f_2^2} J_0\left(\frac{k\rho_0}{f_2} \Delta r'\right) \quad (15)$$

From the above equation, it is clear that the correlation function is independent of order m as well as propagation distance z . The speckle size

$$\Delta r' = \frac{2.4f_2}{k\rho_0} \quad (16)$$

is independent of propagation distance z , directly proportional to focal length f_2 , and inversely proportional to ring radius ρ_0 . Thus, we can say that the near field speckles are diffracting and the far field speckles are non-diffracting in nature.

3 Experimental Setup

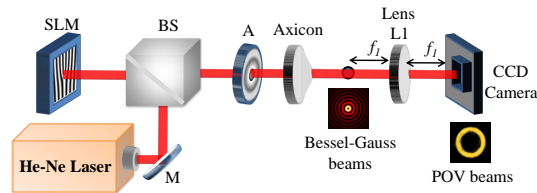


Figure 1. (Colour online) Experimental set up for the generation of POV beams using the Fourier transform of Bessel-Gauss beams (POV generating FT), Where SLM-Spatial Light Modulator, BS-Beam Splitter, A-Aperture, M-Mirror, f_1 -focal length of L1.

The experimental setup designed to generate diffracting and non-diffracting speckles is shown in Fig. 1. We have adopted the method of taking Fourier transform (FT) of Bessel-Gauss (BG) beams to produce the POV beams. Optical vortex beams are initially generated by illuminating a computer generated hologram displayed on a spatial light modulator. The beams then propagate through an axicon of apex angle 178° ^{32,33} to produce BG beams. The Fourier transform of BG beams is taken using a lens of focal length 30 cm, and at the back focal plane we obtain the POV beams (POV generating FT). We use a He-Ne laser of power 5 mW and wavelength 632.8 nm.

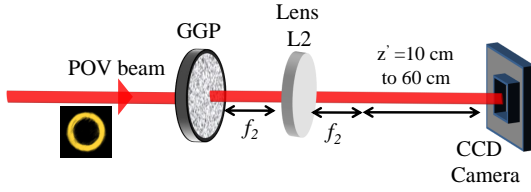


Figure 2. (Colour online) Experimental set up for producing the diverging and non-diverging speckle patterns, Where GGP-Ground Glass Plate, f_2 -focal length of L2 used for speckle FT.

The generated POV beams are scattered through a ground glass plate (DG10-600, from Thorlabs) as shown in Fig. 2. The ground glass plate is placed at the back focal plane of the lens L1 in Fig. 1, i.e. at the origin of POV beams. The near field speckles, without using the lens (L2) of focal length f_2 shown in Fig.2, are recorded just after the GGP. The diverging nature can be verified by looking at the size of the speckles at various distances within the range 20-70 cm from GGP at an interval of 5 cm. For generating the far field speckles, we take the Fourier transform of near field speckles using the lens (L2) placed at a distance of $f_2 = 50\text{cm}$ from the GGP (speckle FT). For recording the POV beams and the corresponding speckles, we use a CCD camera (FLIR) with pixel size $3.14\mu\text{m}$.

4 Results & Analysis

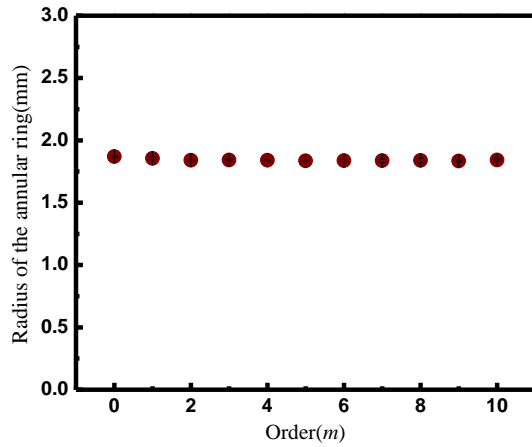


Figure 3. (Colour online) The variation of the radius of the annular ring with the order of experimentally generated POV beams.

We start our experiment by recording the intensity distribution of POV beams at the Fourier plane of lens L1. For verifying the order independent intensity distribution, we have measured the radius of the bright ring for different orders of the POV beam, and the results are shown in Fig. 3. The radius has been calculated by averaging over 20 line profiles (i.e. 40 radii values) taken along diameters in different directions. From the figure, it is clear that the radius is independent of the order and confirms the quality of our POV beams. The average radius of the annular ring of the POV beams is obtained as $\rho_0 = 1.844 \pm 0.013\text{mm}$, which has been used in all our theoretical calculations.

We have recorded the speckle patterns corresponding to different orders of the POV beams by placing a camera immediately after the GGP. Fig 4 shows the speckle patterns obtained by scattering a second order POV beam and observed at different propagation distances $z = 20, 45,$ and 70cm (from left to right). It is evident from the figure that the size of the speckles increases with propagation distance, i.e. the near-field speckles are diverging in nature.

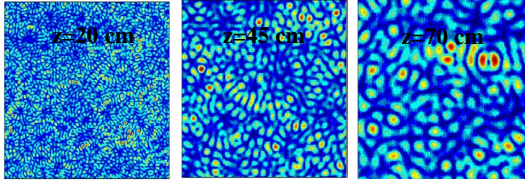


Figure 4. (Colour online) The speckle patterns obtained by the scattering of POV beam of order $m = 2$ at different propagation distances $z=20\text{cm}$, $z=45\text{cm}$ and $z=70\text{cm}$ (from left to right) in the near field.

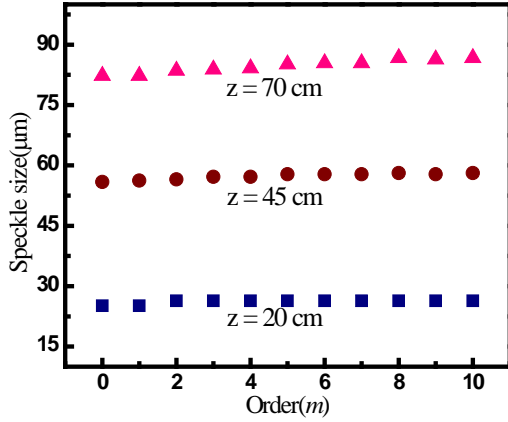


Figure 5. (Colour online) Variation of speckle size with the order of POV beam for different propagation distances $z = 20\text{cm}$ (blue squares), $z = 45\text{cm}$ (red circles), $z = 70\text{cm}$ (pink triangles).

We have also studied the variation of speckle size, obtained as the width of auto-correlation function, with order and found that the size of the speckles is independent of the order of the POV beam. It has been shown graphically in Fig. 5. We have averaged the speckle size at a given propagation distance over 10 samples for each of the 11 orders $m = 0 - 10$.

Figure 6 shows the theoretical (red circles) and experimental (blue triangles) results for the speckle size (now averaged over POV orders) at different propagation distances. From the figure, it is clear that the experimental results are well matching with theoretical values. For finding the theoretical speckle size, we have substituted the experimentally obtained ring radius $\rho_0 = 1.844 \pm 0.013\text{mm}$ in Eq.12. From Fig. 6, one can easily verify that the speckle size varies linearly with propagation distance, which is in agreement with our theoretical results.

We have generated the non-diffracting random fields by taking the Fourier transform of near field speckles (speckle FT), by placing a lens (L2) so that the GGP is in the front focal plane of this lens. Fig. 7 shows the variation of the size of non-diffracting speckles with the propagation distance. It is evident from the figure that the speckle size is invariant with propagation distance and confirms the non-diffracting nature of speckles. Our experimental results are in good agreement with the theoretical calculations, not only in the sense that they are non-diffracting but quantitatively as well.

5 Conclusions

We have proposed a scheme for generating the diffracting as well as non-diffracting speckles by scattering the POV beams. We have also provided the exact analytical expression for near-field and far-field speckle size. It has been proven that the near field speckle size is directly proportional to the propagation distance whereas far-field speckle size is independent of propagation distance. In both cases, the speckle size is independent of the order of the POV beam. We have compared our theoretical results with experimental results and found that they are in good agreement with each other, not only qualitatively but quantitatively. These results may find applications in cryptography and medical optics as we have non-diffracting speckles whose size can be controlled easily by changing the focal length of the lens used to take the Fourier transform of BG beams.

The authors declare no conflicts of interest.

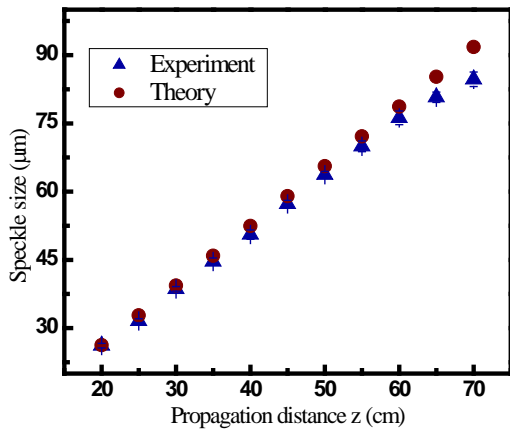


Figure 6. (Colour online) Experimental (blue triangles) and theoretical (red circles) results for the variation of near-field or diverging speckle size with propagation distance.

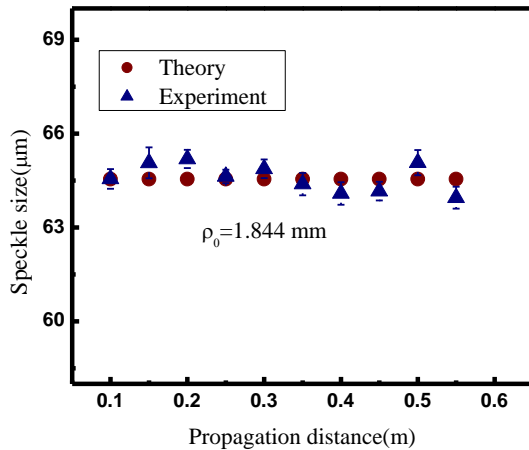


Figure 7. (Colour online) Experimental (blue triangles) and theoretical (red circles) results for the variation of speckle size with propagation distance z .

Acknowledgement

This work was partly supported by JSPS KAKENHI Grant Number JP20H05888. The author SGR acknowledges financial support from DST-SERB through start-up research grant (SRG/2019/000857).

References

1. Heckenberg, N., McDuff, R., Smith, C. & White, A. Generation of optical phase singularities by computer-generated holograms. *Opt. letters* **17**, 221–223 (1992).
2. Torres, J. P. & Torner, L. *Twisted photons: applications of light with orbital angular momentum* (John Wiley & Sons, 2011).
3. Franke-Arnold, S., Allen, L. & Padgett, M. Advances in optical angular momentum. *Laser & Photonics Rev.* **2**, 299–313 (2008).
4. Molina-Terriza, G., Torres, J. P. & Torner, L. Twisted photons. *Nat. physics* **3**, 305–310 (2007).
5. Yao, A. M. & Padgett, M. J. Orbital angular momentum: origins, behavior and applications. *Adv. optics photonics* **3**, 161–204 (2011).
6. Reddy, S. G., Kumar, A., Prabhakar, S. & Singh, R. Experimental generation of ring-shaped beams with random sources. *Opt. letters* **38**, 4441–4444 (2013).

7. Ostrovsky, A. S., Rickenstorff-Parrao, C. & Arrizón, V. Generation of the “perfect” optical vortex using a liquid-crystal spatial light modulator. *Opt. letters* **38**, 534–536 (2013).
8. Chen, M., Mazilu, M., Arita, Y., Wright, E. M. & Dholakia, K. Dynamics of microparticles trapped in a perfect vortex beam. *Opt. letters* **38**, 4919–4922 (2013).
9. Vaity, P. & Rusch, L. Perfect vortex beam: Fourier transformation of a Bessel beam. *Opt. letters* **40**, 597–600 (2015).
10. Gori, F., Guattari, G. & Padovani, C. Bessel-gauss beams. *Opt. communications* **64**, 491–495 (1987).
11. Reddy, S. G., Prabhakar, S., Kumar, A., Banerji, J. & Singh, R. Higher order optical vortices and formation of speckles. *Opt. Lett.* **39**, 4364–4367 (2014).
12. Hu, X.-B., Dong, M.-X., Zhu, Z.-H., Gao, W. & Rosales-Guzmán, C. Does the structure of light influence the speckle size? *Sci. reports* **10**, 1–11 (2020).
13. Goodman, J. W. *Speckle phenomena in optics: theory and applications* (Roberts and Company Publishers, 2007).
14. Dainty, J. C. *Laser speckle and related phenomena*, vol. 9 (Springer science & business Media, 2013).
15. Françon, M. *Laser speckle and applications in optics* (Elsevier, 2012).
16. Jacquot, P. & Fournier, J.-M. *Interferometry in speckle light: Theory and applications* (Springer Science & Business Media, 2012).
17. Ricklin, J. C. & Davidson, F. M. Atmospheric turbulence effects on a partially coherent gaussian beam: implications for free-space laser communication. *JOSA A* **19**, 1794–1802 (2002).
18. Schouten, H. F., Gbur, G., Visser, T. D. & Wolf, E. Phase singularities of the coherence functions in young’s interference pattern. *Opt. letters* **28**, 968–970 (2003).
19. Kumar, P., Fatima, A. & Nishchal, N. K. Image encryption using phase-encoded exclusive-or operations with incoherent illumination. *J. Opt.* **21**, 065701 (2019).
20. Heeman, W. *et al.* Application of laser speckle contrast imaging in laparoscopic surgery. *Biomed. optics express* **10**, 2010–2019 (2019).
21. Sirohi, R. Speckle metrology: Some newer techniques and applications. In *International Trends in Optics and Photonics*, 318–327 (Springer, 1999).
22. Cheng, H. & Duong, T. Q. Simplified laser-speckle-imaging analysis method and its application to retinal blood flow imaging. *Opt. letters* **32**, 2188–2190 (2007).
23. Fercher, A. & Briers, J. D. Flow visualization by means of single-exposure speckle photography. *Opt. communications* **37**, 326–330 (1981).
24. Kermisch, D. Partially coherent image processing by laser scanning. *JOSA* **65**, 887–891 (1975).
25. Reddy, S. G. *et al.* Non-diffracting speckles of a perfect vortex beam. *J. Opt.* **18**, 055602 (2016).
26. Cottrell, D. M., Craven, J. M. & Davis, J. A. Nondiffracting random intensity patterns. *Opt. letters* **32**, 298–300 (2007).
27. Dudley, A. *et al.* Controlling the evolution of nondiffracting speckle by complex amplitude modulation on a phase-only spatial light modulator. *Opt. Commun.* **285**, 5–12 (2012).
28. Vanitha, P. *et al.* Correlations in scattered perfect optical vortices. *J. Opt.* (2021).
29. Goodman, J. W. *Statistical optics* (John Wiley & Sons, 2015).
30. Acevedo, C. H. & Dogariu, A. Non-evolving spatial coherence function. *Opt. letters* **43**, 5761–5764 (2018).
31. Zwillinger, D. & Jeffrey, A. *Table of integrals, series, and products* (Elsevier, 2007).
32. Bezerra, D. O., Amaral, J. P., Fonseca, E. J., Alves, C. R. & Jesus-Silva, A. J. Sorting of spatially incoherent optical vortex modes. *Sci. reports* **10**, 1–7 (2020).
33. Alves, C. R., Jesus-Silva, A. J. & Fonseca, E. J. Using speckles to recover an image after its transmission through obstacles. *Phys. Rev. A* **93**, 043816 (2016).